Chaos, Solitons and Fractals 168 (2023) 113126

Contents lists available at ScienceDirect

Chaos, Solitons and Fractals

journal homepage: www.elsevier.com/locate/chaos

Electromagnetohydrodynamic effects with single-walled carbon nanotubes particles in a corrugated microchannel

Ahmed Y. Sayed [a,*], Shaaban I. Ahmed [b], Khaled S. Mekheimer [c], Mohamed S. Abdel-wahed [b,d]

[a] Department of Engineering Mathematics and Physics, Faculty of Engineering El-Materia, Helwan University, Cairo, Egypt
[b] Department of Basic Engineering Sciences, Faculty of Engineering, BADR University in Cairo BUC, Egypt
[c] Department of Applied Mathematics, Faculty of Science (Boys), Al-Azhar University, Cairo, Egypt
[d] Department of Basic Engineering Sciences, Faculty of Engineering at Benha, Benha University, Cairo, Egypt

ARTICLE INFO

Keywords:
Microchannel
Corrugated walls
Electromagnet-hydrodynamic
Nanofluid
Perturbation method
Electro-osmotic field

ABSTRACT

Single-walled carbon nanotubes (SWCNTs) are an advanced product of nanotechnology with notable mechanical and physical properties. This motivated us to investigate the effect of electromagnetic hydrodynamic (EMHD) flow on SWCNTs suspended in a microchannel with corrugated walls. The corrugation of the wavy walls is described by periodic sinusoidal waves of small amplitudes (ϵ), either in phase or out of phase. The problem simulated with a system of governing equations, such as potential, momentum, and heat equations, which were solved analytically using the perturbation method. The behavior of nanofluid velocity, temperature, volumetric flow rate, and average velocity was investigated using three models of thermal characteristics. The results confirm that, the addition of SWCNTs, reduces the fluid velocity at the center of the channel by providing resistance to the fluid motion. The concentration (ϕ) of SWCNTs influence enhances the rate of heat transfer. Additionally, Xue's model has the highest heat transfer rate compared to Maxwell and Hamilton Crosser's (H-C) models. Finally, the obtained flow rate results were compared with previously published data and found to be in good agreement.

1. Introduction

Recently, many researchers were interested in investigating the impact of nanoparticles due to their new physical and thermophysical properties, as well as how these new features affect the industry and biomedical fields. Choi [1] was the first to investigate the efficacy of heat transfer using nanoparticles, and the concept of nanofluid has started to spread. Khanafer et al. [2] investigated the heat transfer enhancement due to the use of carbon nanotubes in the base fluid inside an enclosure, and according to the results, they deduced that the mechanical and thermodynamic properties had improved. Kakac et al. [3] presented a review of how metal nanoparticles in a base fluid, such as water, improved heat transfer. Furthermore, the review demonstrated the investigation of variables based on the development and presentation of the thermophysical properties of a nanofluid. Wahid et al. [4] investigated the impact of velocity slipping and thermal radiation on the velocity and temperature profiles of magnetohydrodynamic hybrid Cu-Al_2O_3/water nanofluid flow over a stretching sheet. Turkylmazoglu [5] investigated the flow and heat transfer of nanofluid over a rotating disc, taking five different types of nanoparticles into account. They concluded that the nanofluids derived from Cu, CuO, and Ag produce less axial fluid compared with those derived from Al_2O_3 and TiO_2. Moreover, the presence of Cu nanoparticles and a low rate for TiO2 results in a high heat transfer rate. Elsaid and Abdel-wahed [6] presented a numerical case study for the rate of cooling of a moving cylinder into a coolant supported by two types of nanoparticles (Cu/Al_2O_3), they found that using (Al_2O_3-water) +5 % Cu as a coolant is relatively better than using (Cu-water) +5 % Al_2O_3. Abbasi et al. [7] studied the Brownian motion and the thermophoresis of the non-Newtonian nanofluid runs within a peristaltic channel. Sayed and Abdel-wahed [8] examine the effect of the nanoparticle type and its concentration as well as the type of base fluid, whether Newtonian or non-Newtonian, on the rate of entropy generated and the rate of heat flux from the surface of an MHD nanofluid with a microrotation boundary layer over a moving permeable plate, they found that that the entropy generation of the non-Newtonian fluids (fluids with microrotation elements) is higher than that of the Newtonian fluids and that the presence of nanoparticles in the cooling system increases the rate of entropy by 1–4 % according to the type and

* Corresponding author.
E-mail address: AHMED_BADR@m-eng.helwan.edu.eg (A.Y. Sayed).

https://doi.org/10.1016/j.chaos.2023.113126
Received 15 November 2022; Received in revised form 22 December 2022; Accepted 6 January 2023

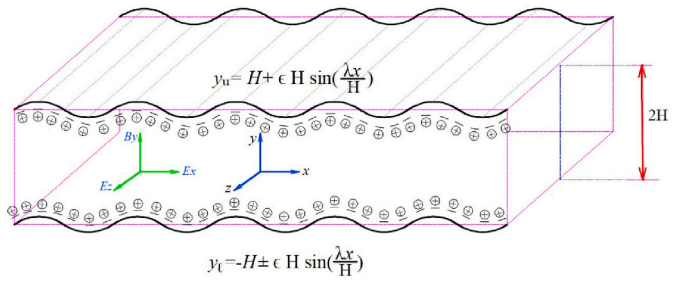

Fig. 1. Geometry of the problem.

concentration of the nanoparticles. Elsaid and Abdel-wahed [9,10] investigated analytically the MHD mixed convection flow of nanofluid inside a vertical channel in the presence/absence of a magnetic induced field. They concluded that an increase in the critical value of the Rayleigh number occur by adding the hybrid nanoparticles within the base fluid. Hayat et al. [11] investigated the mixed convection of peristaltic nanofluid flow runs within a channel, taking two types of nanotubes single and double walls into account. According to the results obtained, adding Single-walled carbon nanotubes (SWCNTs) leads to a decrease in fluid velocity near the center of the channel. Moreover, as the concentration of the SWCNTs increases, the heat transfer rate in the boundary increases. Also, the pressure in the closed section of the pressure leads to a decrease in the pressure rise per wavelength when suspended carbon nanotubes (SWCNTs) are inserted.

Abdel-wahed and Sayed [12] investigated the peristaltic motion of a hybrid/mono-carbon nanotube (SWCNTs)–water flow through a curved channel, they deduce that the hybrid type of nanoparticles raises the pressure gradient at the upper and the lower walls, as well as the heat transfer decreases due to the presence of two types of nanotubes.

Recently, many microfluidic devices have been developed and there have been analytical and numerical models of electromagnetic hydrodynamic (EMHD) flow in microchannels. Chakraborty et al. [13] analyzed the combined effect of magnetic and electric on the fluid flow between two parallel plates. According to the study, a relatively small magnetic field can cause a significant increase in volumetric flow rates. They are, however, highly unreliable in high-strength magnetic fields. Anuar et al. [14] deduced an analytical solution for mixed convection Nano electromagnetohydrodynamic EMHD flow past a vertical sheet, they studied the stability of the deduced solutions for the case of a shrinking sheet. Liu et al. [15] discussed electro-viscous effects on the EMHD flow of Maxwell fluid in a microchannel. They reached an analytical solution and analyzed the flow transport properties concerning the streaming potential and electro-viscous flow. Xue [16] discussed Maxwell's theorem and the methods for determining effective heat, as well as the thermal conductivity of carbon nanotube-based compounds. Zhao et al. [17] analyzed the incompressible viscous Nano electromagnetohydrodynamic flow runs inside a microchannel under the influence of Lorentz force and joule heating, they investigated the behavior of the velocities and heat transfer under the suggested forces. Duwairi and Abdullah [18] studied analytically and numerically the flow and temperature distribution of a hydrodynamic magnetohydrodynamic fluid under the presence of Lorentz force in a micropump. Yoon et al. [19] discussed the effects of wavy surface form, magnetic field, and heat flux from the disc surface of magnetohydrodynamic (MHD) flow across a fast-rotating axisymmetric wavy disc. They also explored the influence of the wavy surface's amplitude on the heat transfer properties of MHD flow across a wavy surface. Buren et al. [20] studied the combined effect of magnetic and electric fields on Jeffrey fluids flowing through a microchannel corrugated wall. Andreozzi et al. [21] investigated the effects of heat transport on nanofluid and ribs in a channel. According to the study, triangular ribs have the best thermal performance. Si and Jian [22] studied the effect of both magnetic and electric fields of the viscous Jeffrey fluid which moves in two parallel corrugated walls under the driven Lorentz force. Rashid et al. [23] investigated the second-grade fluid with a combined effect of magnetic and electric runs between two corrugated walls in a microchannel. Abo-Elkhair et al. [24] examined the use of electric and magnetic fields to control the flow rates of a fluid with variable viscosity moving inside a peristaltic microchannel. Liu et al. [25] investigated the entropy generation rate of the electrohydromagnetic flow of a Newtonian fluid moving through a curved rectangular microchannel. They concluded that the entropy rate increases with the increase of magnetic field parameter *Ha* until a certain value of it then remain constant as *Ha* until the entropy rate attains its maximum value, which occurs at the walls. Rashid and Nadeem [26] analytically investigated the flow of a corrugated microchannel wall with porous media under EMHD effects. They used the perturbation technique to analyze the flow of the second-grade fluid, which they regarded as a working fluid. They explored the flow transport phenomenon without describing the temperature distribution associated with such flow. Reza et al. [27] analytically investigated the effect of hydrodynamic electromagnetic flow supported by nanoparticles in a tiny channel with a uniform undulating rough wall in the presence of an applied magnetic field and a transverse electric field.

From the foregoing description and a detailed literature survey, one can easily conclude that no attempt has been made so far in analyzing the MHD flow of carbon nanotubes immersed in water through a corrugated channel. Thermal conductivity has been studied using a variety of models of Carbon nanotubes (SWCNTs), such as Xue's, Maxwell, and Hamilton-Crosser's (H-C) models because of their importance in the fields of engineering and medicine.

Carbon nanotubes exhibit various characteristic properties such as high thermal conductivity and the improved thermal performance would be applied to energy systems. The system of the governing equations is affected by the Lorenz force, which is created by the interaction of electric and magnetic fields. The perturbation strategy has been used to address the problem in the micro-channel. And the investigation of the features of fluid flow speed and temperature in a tiny channel with corrugated walls, where the two walls are small-amplitude periodic sinusoidal waves that are either in phase or half-period out of phase.

2. Essential equations as well as the mathematical conceptualization

Consider a laminar, Newtonian, incompressible EMHD flow between two immovable corrugated walls with height 2*H*. The origin of the coordinate system is believed to be fixed in the middle of the channel. The layer thickness, *W*, $L \gg 2H$, is substantially more than the width of the channel along the *x*-axis and the length along the *z*-axis (see Fig. 1). The top and lower wavy walls are situated at

$$y_u = H + \varepsilon H \sin\left(\frac{\lambda x}{H}\right), \text{and } y_l = -H \pm \varepsilon H \sin\left(\frac{\lambda x}{H}\right), \tag{1}$$

respectively, where λ is the wave number and ε is small amplitude,

2.1. Electric potential distribution

To calculate the net charge density ρ_e in the Electric Debye length (EDL) in a corrugated wall channel, first we calculate the EDL potential $\Phi^* = \Phi^*(x,y)$. Then $E = -\nabla\Phi^*$, $\nabla \bullet E = \frac{\rho_e}{\epsilon_0}$ gives Poisson's equation $\nabla^2\Phi^* = -\frac{\rho_e}{\epsilon_0}$. Thus,

$$\rho_e = -\epsilon_0\nabla^2\Phi^* = -2ez_0n_0 sinh\frac{ez_0\Phi^*}{k_BT_a}, \tag{2}$$

where $n_0, e_0, z_0,$ and k_B denote the ion density, electronic charge, valence, and Boltzmann constant, respectively. T_a And $\epsilon_0$denote the

Table 1
The Thermophysical properties of the base fluid and nanoparticles [10].

Property	Base fluid/water	SWCNTs
Density (kg/m^3)	997.1	2200
Thermal conductivity (W/mk)	0.613	2200
Specific heat (j/kgK)	4179	709
Thermal expansion coefficient (1/k)10^{-6}	210	15

Table 2
Comparison of numerical values of volumetric flow rate for different Hartmann number (Ha).

Ha	Buren et al. [20]		Reza et al. [27]		Present work	Present work
	$q(1)$	$q(60)$	$q(1)$	$q(60)$	$q(1)$	$q(60)$
0	0.32990	0.33300	0.33090	0.33306	0.33327	0.33328
0.01	0.32970	0.33290	0.33010	0.33330	0.33330	0.33331
0.5	0.30304	0.30299	0.30309	0.30300	0.30305	0.30306
0.75	0.27220	0.27223	0.27220	0.27227	0.27223	0.27223
1	0.23840	0.23846	0.23839	0.23843	0.23839	0.23840
2	0.12950	0.12950	0.12948	0.12950	0.12949	0.12949
5	0.03201	0.03205	0.03199	0.03201	0.03200	0.03200

absolute temperature and the solution's permittivity constant, respectively. Suppose Φ^* is very small. Then $\left(\frac{ez_0\Phi^*}{k_BT_a}\right) \ll 1$ so the term $\left(\frac{ez_0\Phi^*}{k_BT_a}\right)$ can be used to approximate the term $\left(sinh\frac{ez_0\Phi^*}{k_BT_a}\right)$ [27,28]. This principle is known as the Debye–Hückle linearization. Finally, the linearized Poisson equation is obtained in the following form.

$$\nabla^2\Phi^* = \frac{2n_0e^2z_0^2}{\epsilon_0k_BT_a}\Phi^*, \tag{3}$$

where $k = ez_0\sqrt{\frac{2n_0}{\epsilon_0k_BT_a}}$ is the Debye–Hückle parameter [27]. Then

$$\nabla^2\Phi^* = k^2\Phi^*. \tag{4}$$

And the boundary conditions are

$$\Phi^* = \zeta l \quad at\ y_u = H + \varepsilon\, H\, sin\left(\frac{\lambda\, x^*}{H}\right), y_l = -H \pm \varepsilon\, H\, sin\left(\frac{\lambda\, x^*}{H}\right).$$

Also, the non-dimensional variables are defined as

$$\Phi = \frac{\Phi^*}{\zeta}, y = \frac{y^*}{H}, x = \frac{x^*}{H}.$$

Assume that the ζ potential is constant. To make dimensionless the linearized Poisson equation, we substitute the non-dimensional variables into Eq. (4) to get

$$\nabla^2\Phi = \alpha^2\Phi \tag{5}$$

where $\alpha = kH$ is the normalized reciprocal thickness of the EDL, which denotes the ratio of the microchannel's half height to Debye length $\left(\frac{1}{k}\right)$.

The dimensionless boundary conditions for the electrical potential are defined as:

$$\Phi = 1 \quad at\ y = 1 + \varepsilon\, sin(\lambda\, x), \tag{6}$$

$$\Phi = 1\ at\ y = -1 \pm \varepsilon\, sin(\lambda\, x). \tag{7}$$

The electric potential function can be described by the regular perturbation expansion in small values of ε [18,27].

$$\Phi(x,y) = \Phi_o(x,y) + \varepsilon\,\Phi_1(x,y) + \varepsilon^2\Phi_2(x,y) + \bullet\bullet\bullet\bullet\bullet\bullet\bullet\bullet\bullet\bullet\bullet\bullet\bullet\bullet\bullet. \tag{8}$$

By substituting Eq. (8) into Eq. (5), we get

Table 4
Typical values of the physical variables [26].

Physical variables	Values [units]
Characteristic channel length (H)	40 μm
Charge of the photon (e)	1.6×10^{-19} Coulomb
Electrical potential at the wall (ξ)	-12 Vm
Electrical field in axial direction (E_x)	$0-2\times10^4$ V/m
Electrical field in transverse direction (E_z)	$0-2\times10^4$ V/m
Applied magnetic field (B_y)	1–50 T
Boltzmann constant (k_B)	1.38×10^{-23} J/K
Ion density (n_0)	1 mol/m^3
Average absolute temperature (T_a)	300 K
Initial surface temperature (T_w)	300 K
Valence of ions (z)	1
Permittivity of the fluid (ϵ_0)	5.3×10^{-10} C/Vm
Viscosity of the fluid (μ)	$10-6$ m^2/s
Permeability of porous media (K)	$0-10^{-11}$ m^2
Electrical conductivity (σ_e)	1000 W/m^2

Table 5
Numerical values of the Nusselt number rate at the upper wall for different values of concentration.

ϕ	$x=0$	% of incensement	$x=60$	% of incensement
Maxwell's model				
0.05	2.08136	–	1.24011	–
0.1	2.20113	5.75%	1.36624	10.17%
0.15	2.42342	10.10%	1.56301	14.40%
0.2	2.78712	15.01%	1.86028	19.02%
(H-C) model				
0.05	2.01712	–	1.19202	–
0.1	2.03471	0.87%	1.24167	4.17%
0.15	2.09627	3.03%	1.31812	6.16%
0.2	2.20502	5.19%	1.42455	8.07%
Xue's model				
0.05	2.63781	–	1.65664	–
0.1	3.34464	26.80%	2.22224	34.14%
0.15	4.17600	24.86%	2.87494	29.37%
0.2	5.15013	23.33%	3.62915	26.23%

Table 3
The volumetric flow rate for different concentration of nanoparticles ϕ on corrugated walls.

Ha	$\phi=0.05$		$\phi=0.1$		$\phi=0.2$	
	$q(1)$	$q(60)$	$q(1)$	$q(60)$	$q(1)$	$q(60)$
0	0.2932044	0.2932158	0.2561344	0.2561443	0.1908035	0.1908109
0.01	0.2931931	0.2932045	0.2561248	0.2561348	0.1907972	0.1908045
0.5	0.2671459	0.2671554	0.2340579	0.2340662	0.1757719	0.1757782
0.75	0.2404958	0.2405035	0.2113437	0.2113504	0.1600461	0.1600513
1	0.2111077	0.2111136	0.1861343	0.1861396	0.1422766	0.1422807
2	0.1155396	0.1155414	0.1029685	0.1029701	0.0811838	0.0811851
5	0.0287378	0.0287379	0.0258518	0.0258519	0.0209661	0.0209661

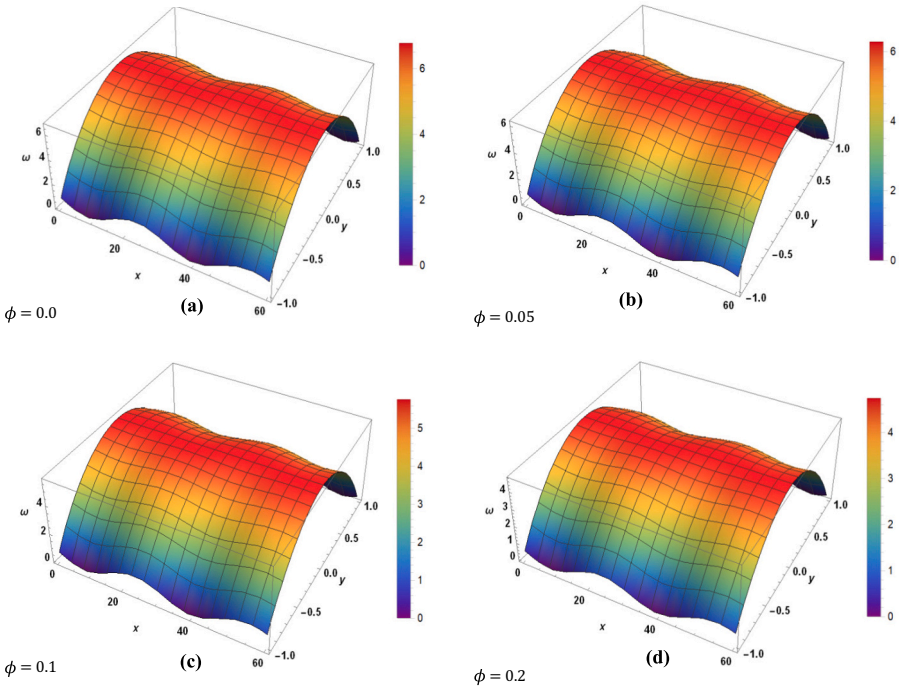

Fig. 2. The velocity distribution in three dimensions for (same phase) $\varepsilon = 0.05, \lambda = 0.2, \alpha = 10, S = 25, Ha = 0.5$.

$$\varepsilon^0: \quad \frac{\partial^2 \Phi_0}{\partial x^2} + \frac{\partial^2 \Phi_0}{\partial y^2} - \alpha^2 \Phi_0 = 0, \tag{9}$$

$$\varepsilon^1: \quad \frac{\partial^2 \Phi_1}{\partial x^2} + \frac{\partial^2 \Phi_1}{\partial y^2} - \alpha^2 \Phi_1 = 0, \tag{10}$$

$$\varepsilon^2: \quad \frac{\partial^2 \Phi_2}{\partial x^2} + \frac{\partial^2 \Phi_2}{\partial y^2} - \alpha^2 \Phi_2 = 0. \tag{11}$$

In a Taylor series concerning the mean wall positions $y = 1$ and $y = -1$, the boundary constraints Eqs. (6) and (7) can be expanded in the following form

$$1 = \Phi(x,1) + \varepsilon sin(\lambda x) \frac{\partial \Phi}{\partial y}(x,1) + \frac{\varepsilon^2}{2} sin^2(\lambda x) \frac{\partial^2 \Phi}{\partial y^2}(x,1) + \bullet\bullet\bullet\bullet\bullet\bullet\bullet\bullet\bullet\bullet\bullet\bullet\bullet, \tag{12}$$

$$1 = \Phi(x,-1) \pm \varepsilon sin(\lambda x) \frac{\partial \Phi}{\partial y}(x,-1) + \frac{\varepsilon^2}{2} sin^2(\lambda x) \frac{\partial^2 \Phi}{\partial y^2}(x,-1) + \bullet\bullet\bullet\bullet\bullet\bullet\bullet\bullet\bullet\bullet\bullet\bullet\bullet. \tag{13}$$

Similarly, the corresponding boundary conditions Eqs. (9), (10), and (11), can be simplified further by collecting terms of equal powers, respectively as follows.

$$\varepsilon^o: \left\{ \Phi_o(x,y)\big|_{y=1} = 1\,,\ \Phi_o(x,y)\big|_{y=-1} = 1 \right. \tag{14}$$

$$\varepsilon^1: \begin{cases} \Phi_1(x,y)\big|_{y=1} + sin(\lambda x) \left.\dfrac{\partial \Phi_o(x,y)}{\partial y}\right|_{y=1} = 0, \\ \Phi_1(x,y)\big|_{y=-1} \pm sin(\lambda x) \left.\dfrac{\partial \Phi_o(x,y)}{\partial y}\right|_{y=-1} = 0, \end{cases} \tag{15}$$

$$\varepsilon^2: \begin{cases} \Phi_2(x,y)\big|_{y=1} + sin(\lambda x) \left.\dfrac{\partial \Phi_1(x,y)}{\partial y}\right|_{y=1} + \dfrac{sin^2(\lambda x)}{2} \left.\dfrac{\partial^2 \Phi_o(x,y)}{\partial y^2}\right|_{y=1} = 0, \\ \Phi_2(x,y)\big|_{y=-1} \pm sin(\lambda x) \left.\dfrac{\partial \Phi_1(x,y)}{\partial y}\right|_{y=-1} + \dfrac{sin^2(\lambda x)}{2} \left.\dfrac{\partial^2 \Phi_o(x,y)}{\partial y^2}\right|_{y=-1} = 0. \end{cases} \tag{16}$$

From Eqs. (9) and (14), we get

$$\Phi_0^{\pm}(x,y) = \frac{cosh(y\,\alpha)}{cosh(\alpha)}. \tag{17}$$

From Eqs. (10) and (15), we have

$$\therefore \Phi_1^{\pm}(x,y) = -\alpha\, Sin[x\lambda]\, Tanh[\alpha] \begin{cases} \dfrac{\mathrm{Sinh}[yS_1]}{\mathrm{Sinh}[S_1]} & for\ \Phi_1^{+}, \\ \dfrac{\mathrm{Cosh}[yS_1]}{\mathrm{Cosh}[yS_1]} & for\ \Phi_1^{-}. \end{cases} \tag{18}$$

From Eqs. (11) and (16), we get

$$\therefore \Phi_2^{\pm}(x,y) = \frac{1}{4}\alpha\, \mathbf{\Omega_1} \begin{cases} \alpha - \dfrac{2\,S_1 \mathrm{Tanh}[\alpha]}{\mathrm{Tanh}[S_1]} & for\ \Phi_2^{+}, \\ \alpha - \dfrac{2\,S_1 \mathrm{Tanh}[\alpha]}{\mathrm{Coth}[S_1]} & for\ \Phi_2^{-}, \end{cases} \tag{19}$$

where

$$\mathbf{\Omega_1} = \frac{\mathrm{Cos}[2x\lambda]\mathrm{Cosh}[yS_2])}{\mathrm{Cosh}[S_2]} - \frac{\mathrm{Cosh}[y\alpha]}{\mathrm{Cosh}[\alpha]},$$

where S_1, S_2 are defined in Appendix A.

The above Eqs. (9)–(11) with their boundary conditions (14)–(16) are solved exactly using DSolve function with assistance of Mathematica program. By getting $\Phi_o(x,y), \Phi_1(x,y)$, and $\Phi_2(x,y)$, the general solution for the potential equation can be obtained using Eq. (8).

2.2. Velocity distribution

The dimensional form of the continuity and momentum balance

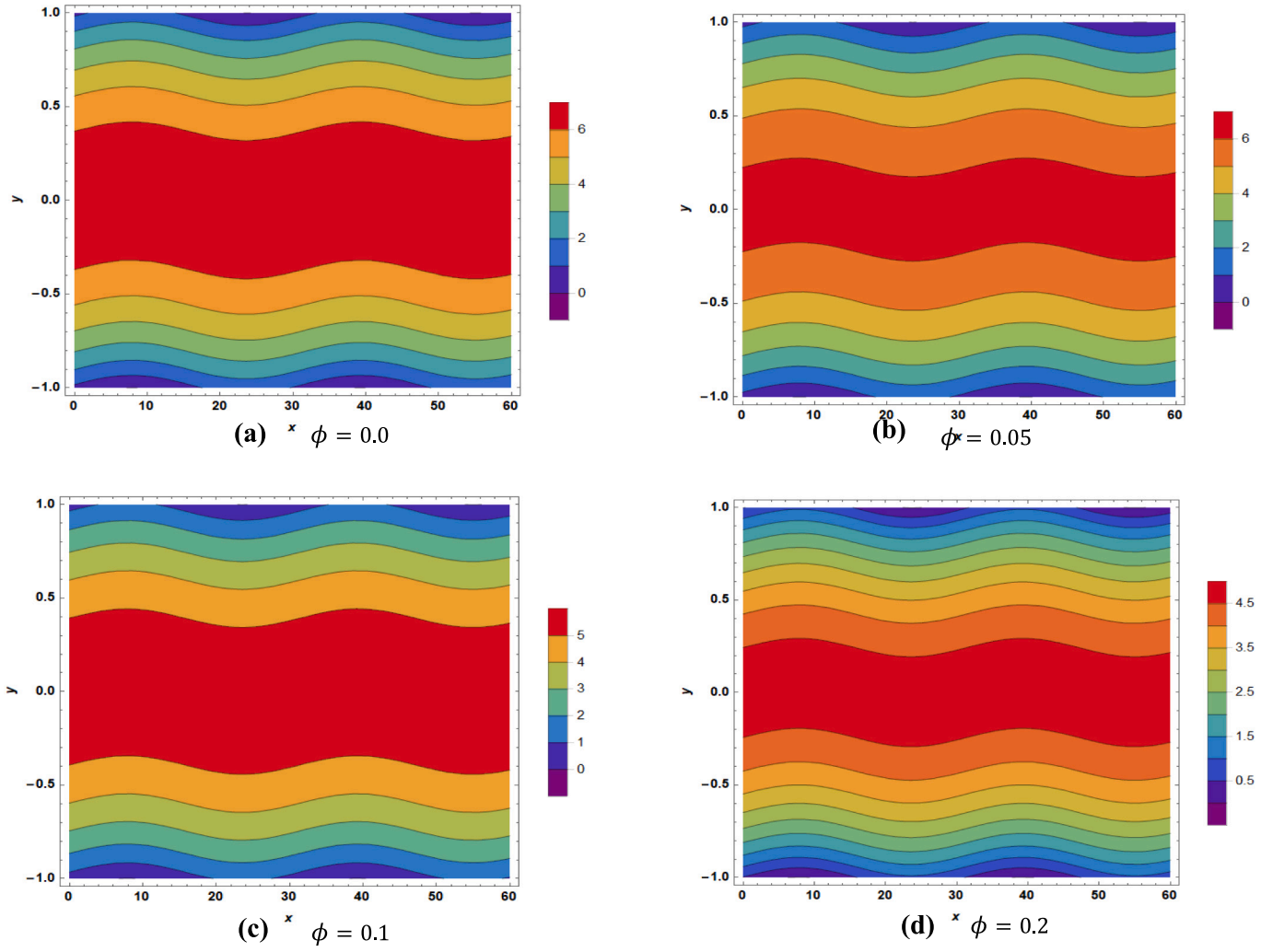

Fig. 3. Contour plot for velocity distribution (same phase) $\varepsilon = 0.05, \lambda = 0.2, \alpha = 10, S = 25, Ha = 0.5$.

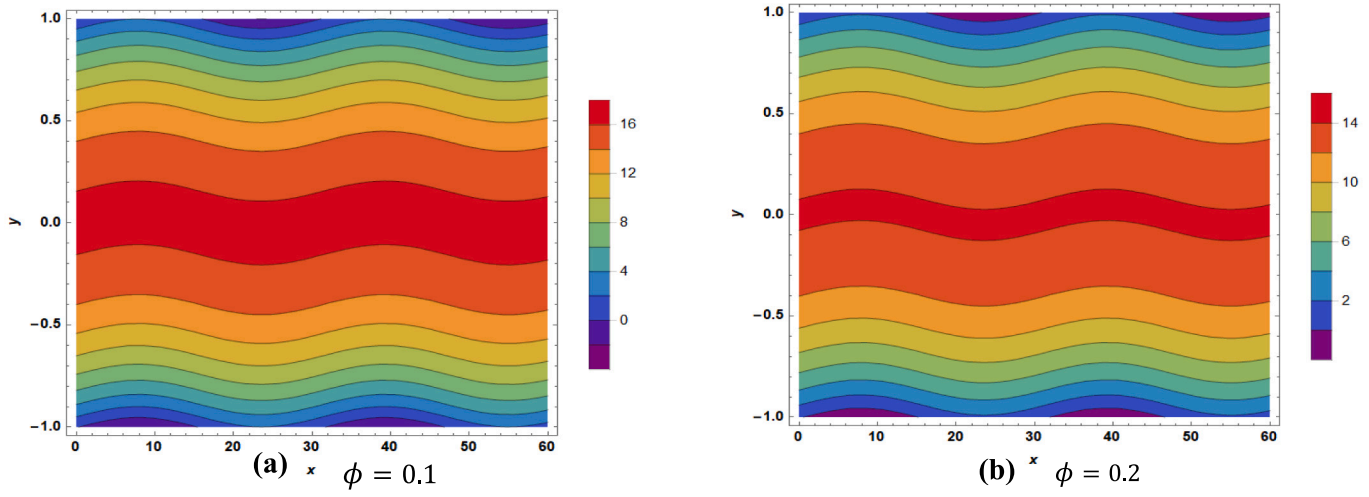

Fig. 4. Contour plot for velocity distribution (same phase) $\varepsilon = 0.05, \lambda = 0.2, \alpha = 10, S = 50, Ha = 1$.

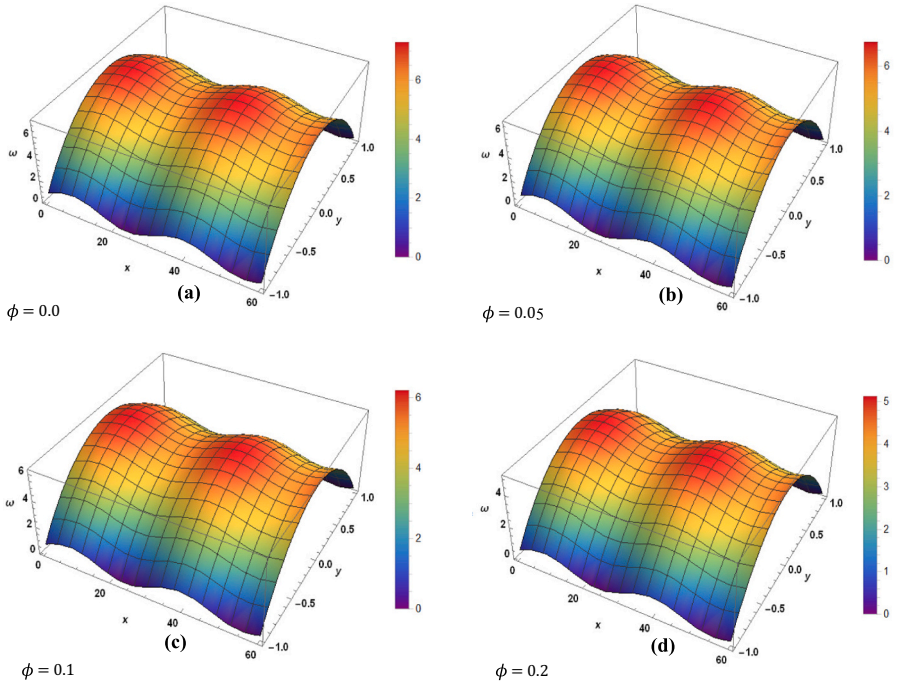

Fig. 5. The velocity distribution in three dimensions for (opposite phase) $\varepsilon = 0.05, \lambda = 0.2, \alpha = 10, S = 25, Ha = 0.5$.

equations for a fluid was given by: [25,29].

$$\rho_{nf}\frac{\partial \vec{u}}{\partial t} + \rho_{nf}(\vec{u} \bullet \nabla)\vec{u} = -\nabla \vec{p} + \mu_{nf}\nabla^2 \vec{u} + \vec{F}, \tag{20}$$

where

$$\vec{F} = \vec{J} \times \vec{B} + \rho_e \vec{E}. \tag{21}$$

In Eq. (21) ρ_e and $\vec{E}$ denote the net electric charge density and applied electric field. F denotes the Lorentz force, which is formed by the interaction of fluid flow and applied magnetic field, where the magnetic field acts in y-direction, $\vec{B} = B_0 \vec{e}_y$ and the uniform electric field is $\vec{E} = E_x \vec{e}_x + E_z \vec{e}_z$ and the electric current density $\vec{J} = \sigma_{nf}\left[\vec{u} \times \vec{B}\right] + \sigma_{nf}\vec{E}$ caused by an x-directional electric field [26]. Therefore, the momentum equation in z-direction takes the form:

$$\mu_{nf}\left(\frac{\partial^2 w^*}{\partial x^{*2}} + \frac{\partial^2 w^*}{\partial y^{*2}}\right) - \frac{\partial \mathrm{P}}{\partial z} - \sigma_{nf} w^* B_o^2 + \sigma_{nf} E_x B_o + \rho_e E_z = 0. \tag{22}$$

By introducing the following Dimensionless variables, and substituting in Eq. (22),

$$x = \frac{x^*}{H}, y = \frac{y^*}{H}, w = \frac{w^*}{V}, Ha^2 = \frac{B_0^2 H^2 \sigma_f}{\mu_f}, p_z = -\frac{H^2}{\mu_f V}\frac{\partial p}{\partial z}, Ha \bullet S$$
$$= B_0 H\sqrt{\frac{\sigma_f}{\mu_f}}, \rho_e = \alpha^2 H^2 \Phi,$$

where

$$\mu_{nf} = \frac{\mu_f}{(1-\phi)^{2.5}}, \sigma_{nf} = \sigma_f\left[1 + \frac{3\,\phi\left(\frac{\sigma_s}{\sigma_f} - 1\right)}{\left(\frac{\sigma_s}{\sigma_f} + 2\right) - \phi\left(\frac{\sigma_s}{\sigma_f} - 1\right)}\right],$$

where ϕ the nanoparticles volume fraction, $A_1 = \frac{\mu_{nf}}{\mu_f}, A_2 = \frac{\sigma_{nf}}{\sigma_f}$, as in [11]. The thermo-physical properties of the base fluid and nanoparticles are listed in Table 1

$$\frac{\partial^2 w}{\partial x^2} + \frac{\partial^2 w}{\partial y^2} - \frac{A_2}{A_1}Ha^2\, w + \frac{\alpha^2}{A_1}\,\Phi = -\frac{1}{A_1}P_z - \frac{A_2}{A_1}Ha^* S, \tag{23}$$

where the Hartmann number (Ha) describes the ratio of Lorentz force to viscous force, and S denotes the transverse electric field, with the following boundary conditions:

$$w = 0\ at. \therefore y_u = 1 + \varepsilon\ sin(\lambda x), \tag{24}$$

$$w = 0\ at. \therefore y_L = -1 \pm \varepsilon\ sin(\lambda x). \tag{25}$$

Using the following transformation in Eq. (23), we obtain

$$u = -\frac{A_2}{A_1}Ha^2 w + \frac{\frac{\alpha^2}{A_1}\,Ha^2}{\left(Ha^2 - \frac{A_1}{A_2}\alpha^2\right)}\Phi. \tag{26}$$

One can deduce the following form of the velocity equation

$$\frac{\partial^2 u}{\partial x^2} + \frac{\partial^2 u}{\partial y^2} - \frac{A_2}{A_1}\,Ha^2 u = Ha^2\frac{A_2}{A_1^2}\,P_z + \frac{A_2^2}{A_1^2}Ha^3 S, \tag{27}$$

By defining the following variables

$$A^2 = \frac{A_2}{A_1}\,Ha^2, Q = \frac{\frac{\alpha^2}{A_1}\,Ha^2}{\left(Ha^2 - \frac{A_1}{A_2}\alpha^2\right)},$$

The boundary conditions take the form

$$u = Q\ at\ y_u = 1 + \varepsilon\ sin(\lambda x) \tag{28}$$

$$u = Q\ at\ y_u = -1 \pm \varepsilon\ sin(\lambda x) \tag{29}$$

The fluid velocity can be described by a regular perturbation expansion in small values of ε [25–27].

$$u(x,y) = u_o(x,y) + \varepsilon\, u_1(x,y) + \varepsilon^2 u_2(x,y) + \bullet\bullet\bullet\bullet\bullet\bullet\bullet\bullet\bullet\bullet\bullet\bullet\bullet\bullet\bullet \tag{30}$$

The differential equations for powers of ε are obtained by substituting Eq. (30) into Eq. (27).

$$\varepsilon^o: \quad \frac{\partial^2 u_o}{\partial x^2} + \frac{\partial^2 u_o}{\partial y^2} - A^2\, u_o = B_1 \tag{31}$$

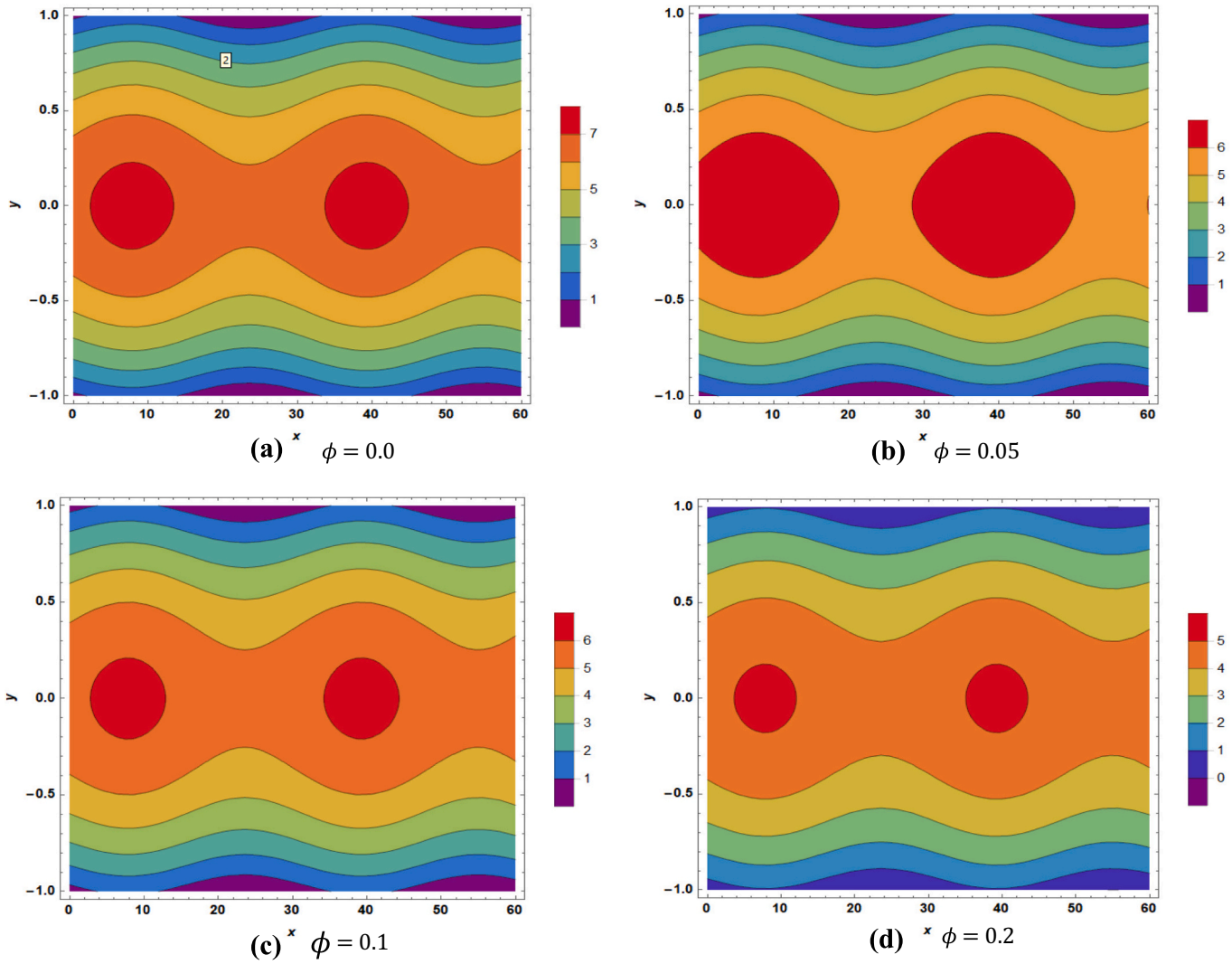

Fig. 6. Contour plot for velocity distribution (opposite phase) $\varepsilon = 0.05, \lambda = 0.2, \alpha = 10, S = 25, Ha = 0.5$.

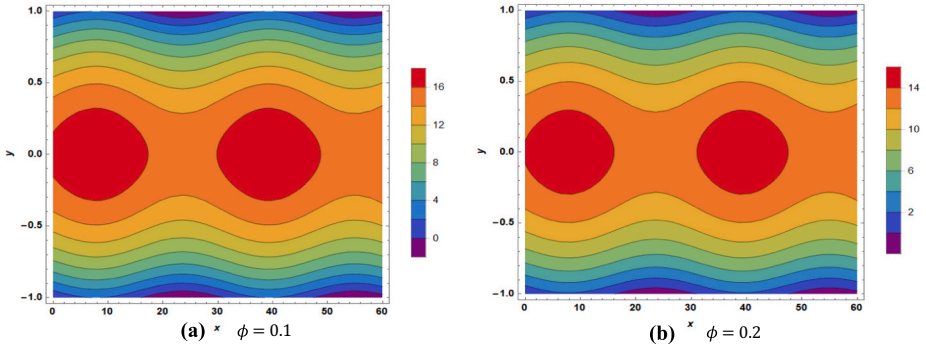

Fig. 7. Contour plot for velocity distribution (opposite phase) $\varepsilon = 0.05, \lambda = 0.2, \alpha = 10, S = 50, Ha = 1$.

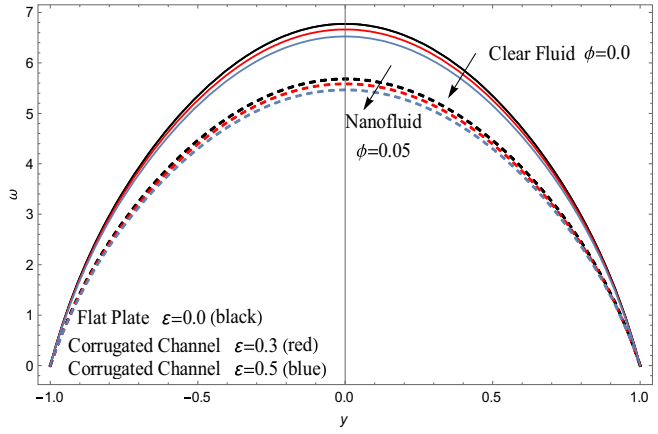

Fig. 8. The velocity distribution for clear/nanofluid at $\varepsilon = 0, \varepsilon = 0.3, \varepsilon = 0.5$.

$$\varepsilon^1: \quad \frac{\partial^2 u_1}{\partial x^2} + \frac{\partial^2 u_1}{\partial y^2} - A^2\, u_1 = 0 \tag{32}$$

$$\varepsilon^2: \quad \frac{\partial^2 u_2}{\partial x^2} + \frac{\partial^2 u_2}{\partial y^2} - A^2\, u_2 = 0 \tag{33}$$

In a Taylor series concerning the mean wall positions $y = 1$ and $y = -1$, the boundary constraints (28) and (29) can be expanded to be in the form:

$$Q = u(x,1) + \varepsilon sin(\lambda\, x)\, \frac{\partial u}{\partial y}(x,1) + \frac{\varepsilon^2}{2} sin^2(\lambda\, x)\, \frac{\partial^2 u}{\partial y^2}(x,1) + \bullet\bullet\bullet\bullet\bullet\bullet\bullet\bullet\bullet\bullet\bullet\bullet\bullet, \tag{34}$$

$$Q = u(x,-1) \pm \varepsilon sin(\lambda\, x)\, \frac{\partial u}{\partial y}(x,-1) + \frac{\varepsilon^2}{2} sin^2(\lambda\, x)\, \frac{\partial^2 u}{\partial y^2}(x,-1) + \bullet\bullet\bullet\bullet\bullet\bullet\bullet\bullet\bullet\bullet\bullet\bullet\bullet. \tag{35}$$

We obtain for the corresponding boundary condition Eqs. (31), (32), and (33), respectively, by collecting terms of equal powers of ε.

$$\varepsilon^o: \left\{ u_o(x,y)\,|_{y=1} = Q\,, u_o(x,y)\,|_{y=-1} = Q\,, \right. \tag{36}$$

$$\varepsilon^1: \begin{cases} u_1(x,y)\,|_{y=1} + sin(\lambda\, x)\, \dfrac{\partial u_o(x,y)}{\partial y}\Big|_{y=1} = 0, \\ u_1(x,y)\,|_{y=-1} \pm sin(\lambda\, x)\, \dfrac{\partial u_o(x,y)}{\partial y}\Big|_{y=-1} = 0, \end{cases} \tag{37}$$

$$\varepsilon^2: \begin{cases} u_2(x,y)\,|_{y=1} + sin(\lambda\, x)\, \dfrac{\partial u_1(x,y)}{\partial y}\Big|_{y=1} + \dfrac{sin^2(\lambda\, x)}{2}\, \dfrac{\partial^2 u_o(x,y)}{\partial y^2}\Big|_{y=1} = 0, \\ u_2(x,y)\,|_{y=-1} \pm sin(\lambda\, x)\, \dfrac{\partial u_1(x,y)}{\partial y}\Big|_{y=-1} + \dfrac{sin^2(\lambda\, x)}{2}\, \dfrac{\partial^2 u_o(x,y)}{\partial y^2}\Big|_{y=-1} = 0. \end{cases} \tag{38}$$

From Eqs. (31) and (36), we derived

$$u_0^{\pm}(x,y) = \frac{e^{-Ay}\left(A^2 e^A (1+e^{2Ay})Q + \left(e^A - e^{Ay} - e^{A(2+y)} + e^{A+2Ay}\right)B_1\right)}{A^2(1+e^{2A})}. \tag{39}$$

From Eqs. (32) and (37), we derived

$$u_1^{\pm}(x,y) = -B_4 \mathrm{Sin}[x\lambda] \begin{cases} \dfrac{\mathrm{Sinh}[yB_2]}{\mathrm{Sinh}[B_2]} & for\ u_1^{+}. \\ \dfrac{\mathrm{Cosh}[yB_2]}{\mathrm{Cosh}[B_2]} & for\ u_1^{-}, \end{cases} \tag{40}$$

From Eqs. (33) and (38), we derived

$$u_2^{\pm}(x,y) = \frac{1}{4}\Omega_2 \begin{cases} \left(A^2 Q + B_1 - \dfrac{2B_2 B_4}{\mathrm{Tanh}[B_2]}\right) for\ u_2^{+}, \\ \left(A^2 Q + B_1 - \dfrac{2B_2 B_4}{\mathrm{Coth}[B_2]}\right) for\ u_2^{-}, \end{cases} \tag{41}$$

where

$$\Omega_2 = \left(\frac{-\mathrm{Cosh}[Ay]}{\mathrm{Cosh}[A]} + \frac{\mathrm{Cos}[2x\lambda]\mathrm{Cosh}[yB_3]}{\mathrm{Cosh}[B_3]}\right).$$

The volume flow rate per unit channel width can be written, where in the last two integrals the function w is expanded in a Taylor series about the mean wall positions. The result is obtained by averaging over one wavelength of corrugations.

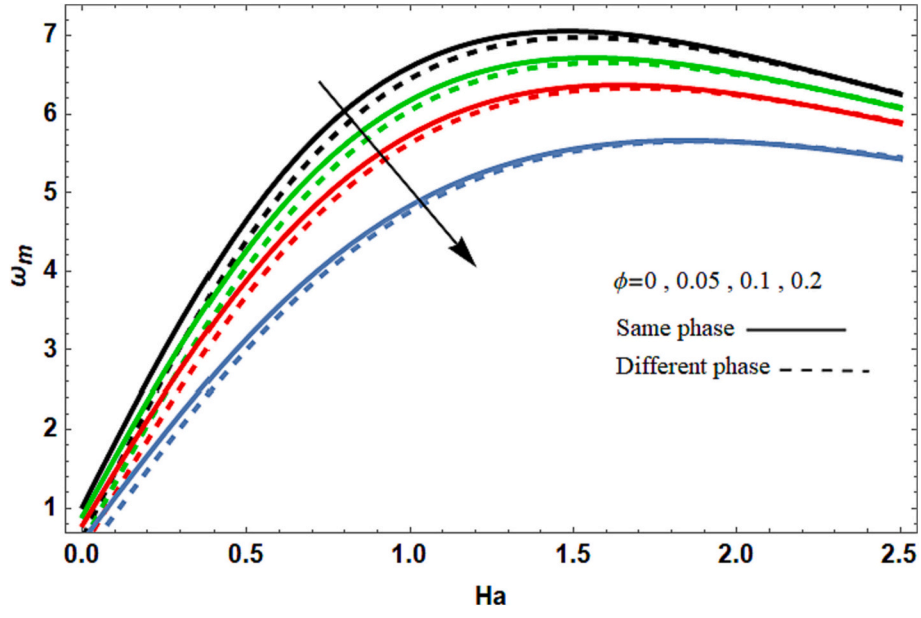

Fig. 9. The Mea velocity w_m and Hartmann number (Ha) for $\varepsilon = 0.2, \lambda = 0.2, \alpha = 10, S = 50$.

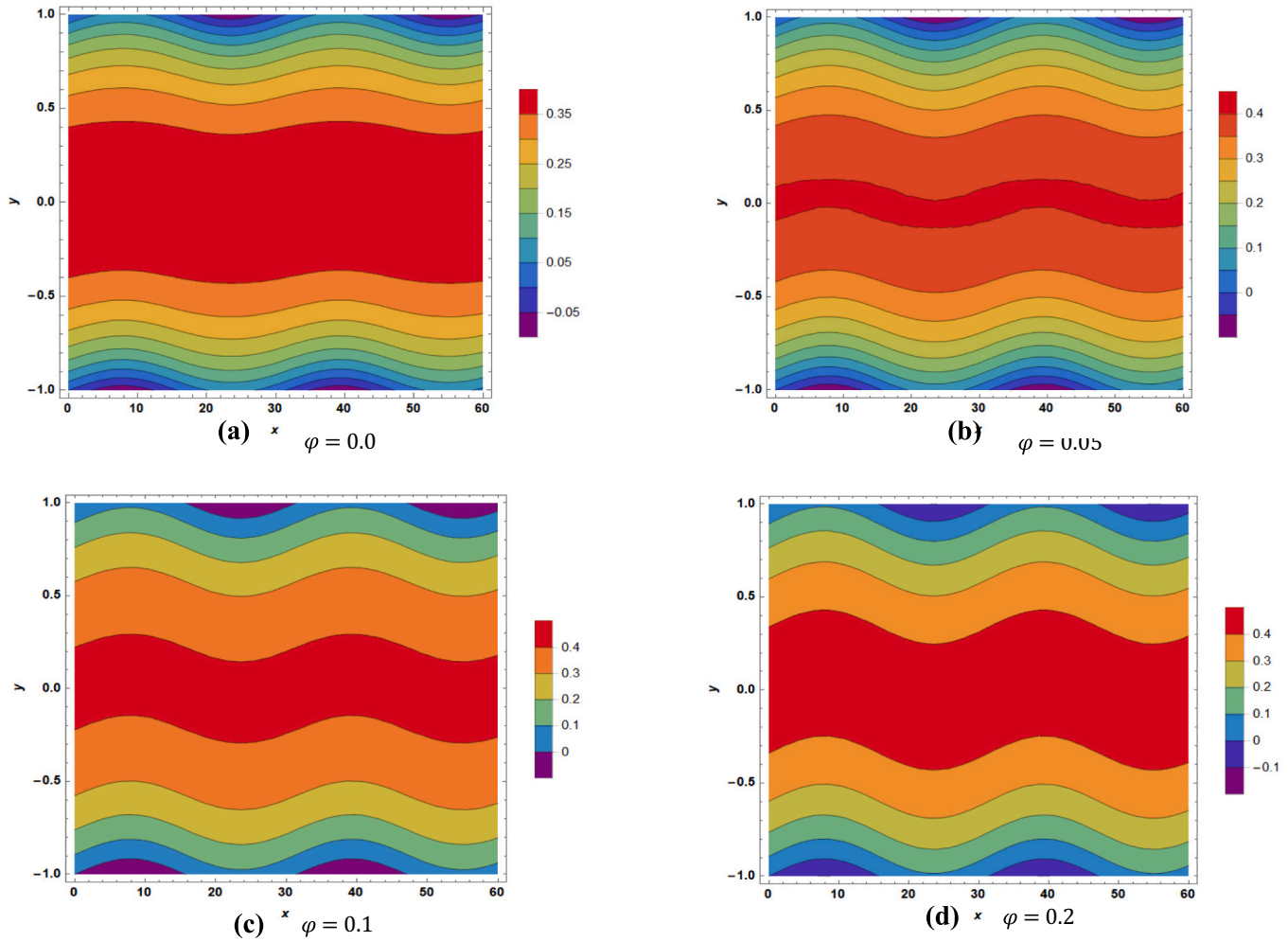

Fig. 10. Contour plot for Temperature distribution (same phase) $\varepsilon = 0.1, \lambda = 0.2, \alpha = 10, S = 25, Ha = 0.5, j = 1, \epsilon = 1$.

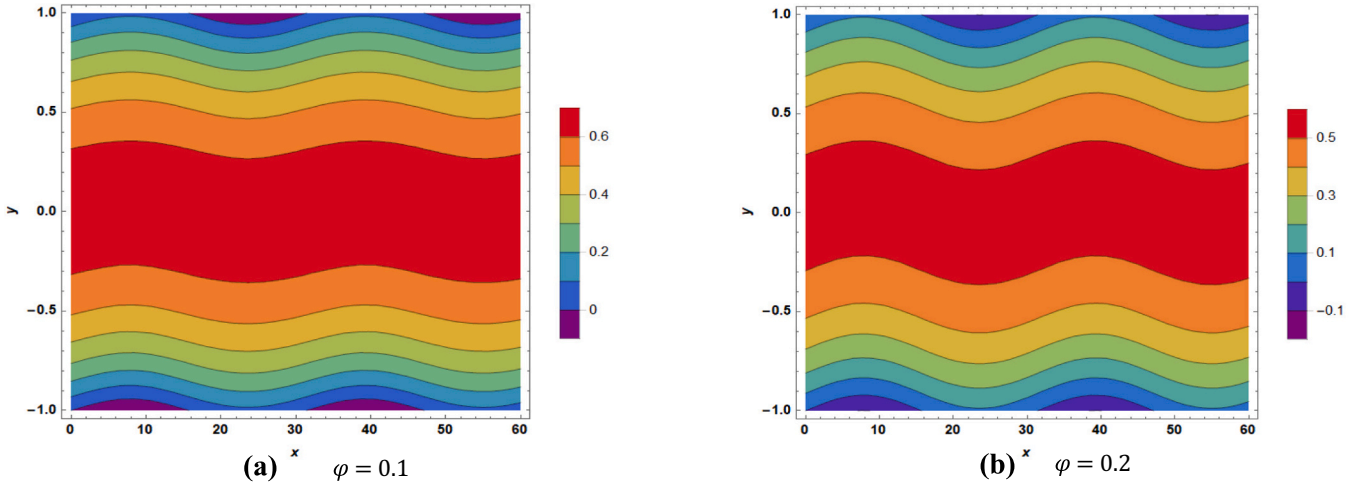

Fig. 11. Contour plot for Temperature distribution (same phase) $\varepsilon = 0.1, \lambda = 0.2, \alpha = 10, S = 50, Ha = 1, j = 1, \epsilon = 1$.

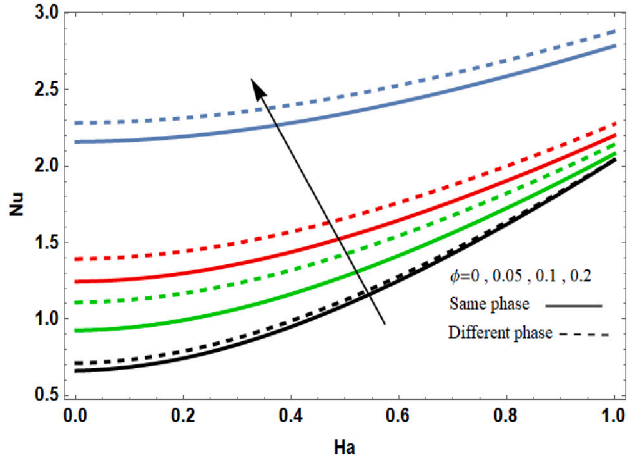

Fig. 12. Variation of *Nu* with *Ha* for different values of ϕ at $\varepsilon = 0.1, \lambda = 0.1, \alpha = 10, S = 25$.

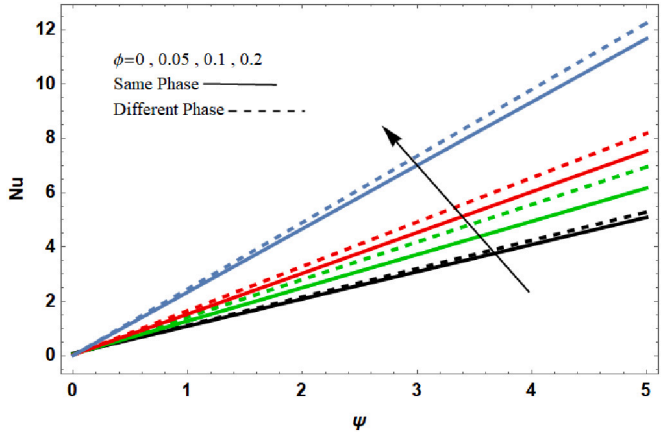

Fig. 13. Variation of *Nu* with heat generation/absorption ψ for different values of ϕ at $\varepsilon = 0.1, \lambda = 0.1, \alpha = 10, S = 25$.

$$q^{\pm}(x) = \int_{y_l}^{y_u} w\,dy = \int_{-1}^{1} w\,dy + \int_{1}^{y_u} w\,dy + \int_{y_l}^{-1} w\,dy$$
$$= \int_{-1}^{1} w_0\,dy + \varepsilon\left[\int_{-1}^{1} \mathrm{w}_1^{\pm}\,dy + sin[\lambda\,x](w_0(1) \mp w_0(-1))\right] + \varepsilon^2\left[\int_{-1}^{1} \mathrm{w}_2^{\pm}\,dy + sin[\lambda\,x](w_1(1) \mp w_1(-1)) + \frac{sin^2[\lambda\,x]}{2}\left(\left.\frac{dw_0}{dx}\right|_{y=1} - \left.\frac{dw_0}{dx}\right|_{y=-1}\right)\right] + \bullet\bullet\bullet\bullet\bullet\bullet\bullet\bullet\bullet \quad (42)$$

The mean velocity is given by

$$w_m^{\pm} = \frac{\lambda}{4\,\pi}\int_0^{\frac{2\,\pi}{\lambda}} q^{\pm}(x)\,dx = w_{0m}\left[1 + \varepsilon^2\phi^{\pm} + O(\varepsilon^4)\bullet\bullet\bullet\bullet\bullet\bullet\bullet\bullet\bullet\right], \quad (43)$$

$$w_{0m}^{\pm} = \frac{2\left(\alpha B_1(A - \mathrm{Tanh}[A]) + A^2 Q(-\alpha\mathrm{Tanh}[A] + A\mathrm{Tanh}[\alpha])\right)}{A^5\alpha}, \quad (44)$$

where, $B_1 - B_4$ are defined in Appendix A

2.3. Temperature distribution

In the presence of nanoparticles, we have to investigate the thermal characteristics of the fluid, and their effect on the flow of carbon nanotube particles suspended in water (SWCNTs). In this study the following models were used:

Maxwell's model [30],

$$\frac{k_{nf}}{k_f} = \left[\frac{k_p + 2k_f - 2\phi\,(k_f - k_p)}{k_p + 2k_f + \phi\,(k_f - k_p)}\right]. \quad (45)$$

Hamilton Crosser's (H-C) model [31],

$$\frac{k_{nf}}{k_f} = \left[\frac{k_p + (n-1)k_f - (n-1)\phi(k_f - k_p)}{k_p + (n-1)k_f + \phi(k_f - k_p)}\right]. \quad (46)$$

Xue's model [16],

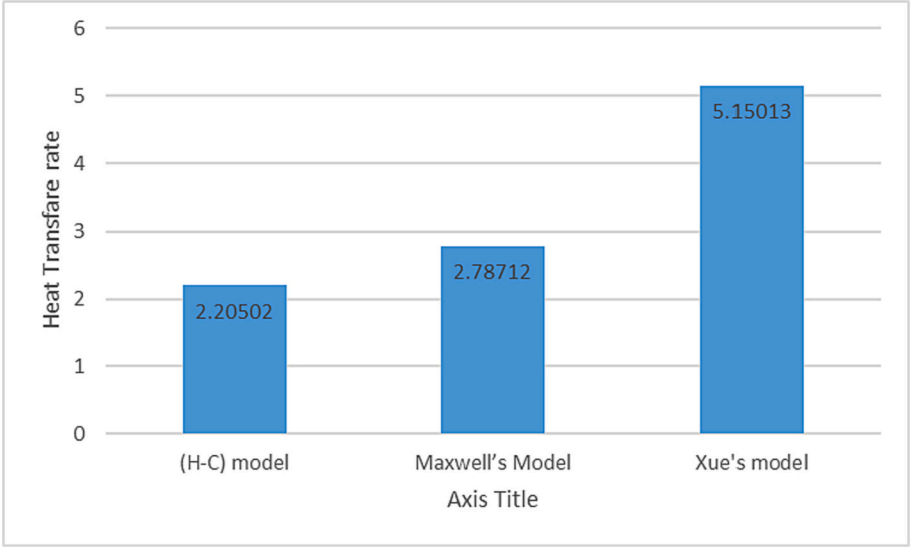

Fig. 14. Heat transfer rate at the wall for different volume fraction of SWCNTs.

$$\frac{k_{nf}}{k_f}=\left[\frac{1-\phi+2\phi\,\frac{k_{CNT}}{k_{CNT}-k_f}ln\left(\frac{k_{CNT}+k_f}{2k_f}\right)}{1-\phi+2\phi\,\frac{k_f}{k_{CNT}-k_f}ln\left(\frac{k_{CNT}+k_f}{2k_f}\right)}\right]. \tag{47}$$

In the above equations, $k_f$denotes the base fluid's thermal conductivity, k_{nf} denotes the nanofluids actual thermal conductivity, k_p denotes the thermal conductivity of nanoparticles, k_{CNT} denotes the thermal conductivity of SWCNTs, and ϕ denotes the nanotubes volume fraction.

Hence, the thermal transport characteristics [6] associated with this model and combined with electromagnetohydrodynamic flows through a corrugated microchannel is written as:

$$(\rho\,C_p)_{nf}\left[w^*\frac{\partial T^*}{\partial z^*}\right]=k_{nf}\left(\frac{\partial^2 T^*}{\partial x^{*2}}+\frac{\partial^2 T^*}{\partial y^{*2}}\right)+J+\psi^*, \tag{48}$$

where T^* *is* the temperature of the fluid, ψ^* is the heat generation/absorption, J is the Joule heating,

$J=\left(E_x^2+E_z^2\right)\sigma_{nf}$, and k_{nf} is the thermal conductivity

The classical non-dimensional temperature is now used for thermally fully evolved flow $T=\frac{k_f(T^*-T_w)}{q_w\,H}$ is now invariant of the axial coordinate for thermally fully developed flow, T_w is the channel wall temperature, which is constant across the cross-section of the channel, q_w is the average inward wall heat flow, of the channel. For thermally fully developed flow with constant heat flux, we may write:

$$\frac{\partial T^*}{\partial z^*}=\frac{\partial T_w^*}{\partial z^*}=\frac{\partial T_b^*}{\partial z^*}, \tag{49}$$

where T_b^* is the bulk mean temperature. The overall energy balance on an element control volume can be expressed as

$$\frac{\partial T_b^*}{\partial z^*}=\frac{q_w}{H\,w_{av}^*(\rho\,C_p)_f}+\frac{J}{w_{av}^*(\rho\,C_p)_f}. \tag{50}$$

Dimensionless variables are created using the non-dimensional variables in Eq. (50).

$$z=\frac{z^*}{H},T=\frac{T^*}{T},w_{0m}=\frac{w_{0m}^*}{u}\text{ and }\frac{k_{nf}}{k_f}=A_4$$

$$(\rho\,C_p)_{nf}=(\rho\,C_p)_f\left(1-\phi+\phi\frac{(\rho\,C_p)_p}{(\rho\,C_p)_f}\right)=A_3(\rho\,C_p)_f, \tag{51}$$

where, $j=\frac{\left(E_x^2+E_z^2\right)\sigma_{nf}\,H}{q_w}$ and $\psi=\left(\frac{H\psi^*}{A_4\,q_w}\right)$

$$\therefore\frac{\partial^2 T}{\partial x^2}+\frac{\partial^2 T}{\partial y^2}-\left(\frac{A_3}{A_4}\right)\left(\frac{w}{w_{0m}}\right)(1+j)=-\frac{1}{A_4}j-\psi, \tag{52}$$

with boundary conditions

$$T=0\;at\;y_u=1+\varepsilon\;sin(\lambda\,x), \tag{53}$$

$$T=0\;at\;y_u=-1\pm\varepsilon\;sin(\lambda\,x) \tag{54}$$

By using the following transformation into the Eq. (52), we have

$$\theta=-\left(\frac{A_4}{A_3}\right)\frac{Ha^2\,u_{av}}{1+j}T+\frac{Ha^2}{A_2\left(Ha^2-\frac{A_1}{A_2}\alpha^2\right)}\Phi. \tag{55}$$

We deduced that

$$\left(\frac{\partial^2\theta}{\partial x^2}+\frac{\partial^2\theta}{\partial y^2}\right)-\frac{A_1}{A_2}u=\left(\frac{1}{A_3}\right)\frac{Ha^2\,u_{av}}{1+j}j+\left(\frac{A_4}{A_3}\right)\frac{Ha^2\,u_{av}}{1+j}\psi, \tag{56}$$

Defining the following variables

$$\gamma=\frac{A_1}{A_2},\delta=\left(\frac{1}{A_3}\right)\frac{Ha^2\,u_{av}}{1+j}j+\left(\frac{A_4}{A_3}\right)\frac{Ha^2\,u_{av}}{1+j}\psi,\beta=\frac{Ha^2}{A_2\left(Ha^2-\frac{A_1}{A_2}\alpha^2\right)}.$$

Then, the boundary conditions take the form

$$\theta=\beta\;at\;y_u=1+\varepsilon\;sin(\lambda\,x), \tag{57}$$

$$\theta=\beta\;at\;y_u=-1\pm\varepsilon\;sin(\lambda\,x). \tag{58}$$

The Temperature function can be described by a regular perturbation expansion in small values of ε [25–27].

$$\theta(x,y)=\theta_o(x,y)+\varepsilon\,\theta_1(x,y)+\varepsilon^2\theta_2(x,y)+\bullet\bullet\bullet\bullet\bullet\bullet\bullet\bullet\bullet\bullet\bullet\bullet\bullet\bullet \tag{59}$$

A differential equation for powers of ε are obtained by substituting Eq. (59) into Eq. (56)

$$\varepsilon^o:\frac{\partial^2\theta_o}{\partial x^2}+\frac{\partial^2\theta_o}{\partial y^2}-\gamma\,u_o=\delta, \tag{60}$$

$$\varepsilon^1:\frac{\partial^2\theta_1}{\partial x^2}+\frac{\partial^2\theta_1}{\partial y^2}-\gamma\,u_1=0, \tag{61}$$

$$\varepsilon^2:\frac{\partial^2\theta_2}{\partial x^2}+\frac{\partial^2\theta_2}{\partial y^2}-\gamma\,u_2=0. \tag{62}$$

In a Taylor series involving the mean wall positions $y=1$ and $y=-1$, the boundary constraints (57) and (58), respectively, can be expanded as follows

$$\beta=\theta(x,1)+\varepsilon sin(\lambda\,x)\,\frac{\partial\theta}{\partial y}(x,1)+\frac{\varepsilon^2}{2}sin^2(\lambda\,x)\,\frac{\partial^2\theta}{\partial y^2}(x,1)+\bullet\bullet\bullet\bullet\bullet\bullet\bullet\bullet\bullet\bullet\bullet\bullet\bullet, \tag{63}$$

$$\beta=\theta(x,-1)\pm\varepsilon sin(\lambda\,x)\,\frac{\partial\theta}{\partial y}(x,-1)+\frac{\varepsilon^2}{2}sin^2(\lambda\,x)\,\frac{\partial^2\theta}{\partial y^2}(x,-1)+\bullet\bullet\bullet\bullet\bullet\bullet\bullet\bullet\bullet\bullet\bullet\bullet. \tag{64}$$

We get for the corresponding boundary condition Eqs. (60), (61), and (62), respectively, by collecting terms of equal powers of ε.

$$\varepsilon^o:\left\{\theta_o(x,y)\,|_{y=1}=\beta\,,\;\theta_o(x,y)\,|_{y=-1}=\beta\,, \right. \tag{65}$$

$$\varepsilon^1:\begin{cases}\theta_1(x,y)\,|_{y=1}+sin(\lambda\,x)\,\dfrac{\partial\theta_o(x,y)}{\partial y}\Big|_{y=1}=0,\\ \theta_1(x,y)\,|_{y=-1}\pm sin(\lambda\,x)\,\dfrac{\partial\theta_o(x,y)}{\partial y}\Big|_{y=-1}=0,\end{cases} \tag{66}$$

$$\varepsilon^2:\begin{cases}\theta_2(x,y)\,|_{y=1}+sin(\lambda\,x)\,\dfrac{\partial\theta_1(x,y)}{\partial y}\Big|_{y=1}+\dfrac{sin^2(\lambda\,x)}{2}\,\dfrac{\partial^2\theta_o(x,y)}{\partial y^2}\Big|_{y=1}=0,\\ \theta_2(x,y)\,|_{y=-1}\pm sin(\lambda\,x)\,\dfrac{\partial\theta_1(x,y)}{\partial y}\Big|_{y=-1}+\dfrac{sin^2(\lambda\,x)}{2}\,\dfrac{\partial^2\theta_o(x,y)}{\partial y^2}\Big|_{y=-1}=0.\end{cases} \tag{67}$$

From Eqs. (60) and (65), we have

$$\begin{aligned}\theta_0^{\pm}(x,y)=&\frac{e^{-Ay}}{2A^4(1+e^{2A})}\left(A^2\left(2\left(e^A-e^{Ay}-e^{A(2+y)}+e^{A+2Ay}\right)Q\gamma\right.\right.\\&+A^2e^{Ay}\left(1+e^{2A}\right)\left(2\beta+\left(-1+y^2\right)\delta\right)\Big)+\left(2e^A+2e^{A+2Ay}\right.\\&\left.\left.+e^{Ay}\left(-2+A^2-A^2y^2\right)+e^{A(2+y)}\left(-2+A^2-A^2y^2\right)\right)\gamma B_1\right)\end{aligned} \tag{68}$$

From Eqs. (61) and (66), we have

$$\theta_1^+(x,y)=g_1{}^+(y)\mathrm{Sin}[x\lambda], \tag{69}$$

$$\theta_1^-(x,y) = g_1{}^-(y)\mathrm{Sin}[x\lambda]. \tag{70}$$

From Eqs. (62) and (67) then

$$\theta_2^+(x,y) = g_2{}^+(y) + f^+(y)Cos[2x\lambda], \tag{71}$$

$$\theta_2^-(x,y) = g_2{}^-(y) + f^-(y)Cos[2x\lambda], \tag{72}$$

where $g_1{}^+(y), g_1{}^-(y), g_2{}^+(y), g_2{}^-(y), f^+(y)$, and $f^-(y)$ are defined in Appendix A.

The Nusselt number, which represents the strength of convective heat exchange, can be calculated as follows

$$Nu^{\pm} = \frac{q^{\pm}(x)\, H}{k_f(T^* - T_w)}, \tag{73}$$

where

$$q^{\pm}(x) = -k_{nf}\left.\frac{\partial T^*}{\partial y^*}\right|_{y^*=y_u^*}. \tag{74}$$

Nusselt number can be written as

$$Nu^{\pm} = -\frac{k_{nf}}{k_f}\left.\frac{\partial T}{\partial y}\right|_{y=y_u}. \tag{75}$$

3. Discussion and outcomes

In this section, the behavior of the fluid supported by (SWCNTs) nanoparticles through corrugated walls is graphically explored. The problem was simulated by a set of partial differential equations and solved analytically using the perturbation method. The approximate analytical solutions were extracted using Mathematica software. The flow rate and heat transfer rate at different points in the microchannel were investigated.

To check the accuracy of the obtained results a comparison with the previously published data under the same conditions is shown in Tables 2 and 3, at $S = 0, \alpha = 0, \phi = 0, P_z = 0.5, \lambda = 0.25$, and $\varepsilon = 0.025$, and the values of non-dimensional parametric variables were calculated according to Table 4 [3,15,27].

It is worth mentioning that the channel's half height is considered to be $H \sim 40\ \mu$m for microfluid inquiry. The effects of the wavy roughness and porous of microchannel on electromagnetically driven flow and temperature were investigated using the following main parametric values [20,27].

$O(\rho) \sim 1 \times 10^3 - 5.91 \times 10^3$ kg m^{-3},

$O(\mu) \sim 0.001$ kg ms^{-1},

$O(By) \sim 1 - 50$T,

$O(Ex)\ 0 - 10^4$ V m^{-1},

$O(Ez) \sim 0 - 10^4$ V m^{-1},

The ranges of all physical variables used in this study are listed in Table 5

$$O(P1) \sim 10\frac{\mathrm{Pa}}{\mathrm{m}},$$

$O(Sj) \sim (-1)\text{–}(-15)$.

3.1. Effect of nanoparticles on the flow velocity

The effect of magnetic field (Hartmann number) on the volumetric flow rate shown in Table 3 for different values of nanoparticle concentration φ. Table 3 shows that the flow rate decreases as the Hartmann number increases under a concentration of nanoparticles owing to the double effect of the body force caused by the applied electromagnetic forces. The first component is the 'flow assist' $\left(\sim \sigma_e E_x B_y\right)$, which is formed between the electric and magnetic fields. The second component is the "opposite flux" $\left(\sim \sigma_e B_y^2 u\right)$, which is controlled by the Lorenz electromagnetic force, and such a force generates a normal component of the velocity while decreasing the main velocity of the flow. However, by investigating the effect of nanoparticle concentration on the flow rate, one can discover that as the nanoparticle concentration increases, the flow rate decreases due to increased fluid viscosity.

Figs. 2 and 3 depict the effect of the nanoparticle concentration on the velocity distribution in three dimensions and contour form for the case of the same phase walls. The velocity is affected only by the surface roughness, when the concentration of carbon particles (SWCNTs) is $\phi = 0.0$, as shown in Figs. 2a and 3a. When a small percentage of carbon particle concentration of $\phi = 0.05$ is added, the physical properties of the liquid were not greatly affected, as shown in Figs. 2b and 3b. and thus, the velocity was affected slightly. In contrast, when the percentage of concentration increased to $\phi = 0.1$ or $\phi = 0.2$ and with the surface roughness, the velocity decreased insignificantly, as shown in Figs. 2c, d, 3c, and d. Fig. 4a and b show the contour plot for the velocity distribution for different values of the nanoparticle concentration at $S = 50$, and $Ha = 1$. When the electric field increases, the velocity increases, and the thickness of the boundary layer increases. Figs. 5 and 6 show the effect of nanoparticle concentration when the phase difference between the two walls is 180°. Figs. 5a and 6a show that the velocity is affected only by the surface roughness, when the concentration of carbon particles (SWCNTs) is $\phi = 0.0$, but the undulating phenomenon occurs because of the phase difference. When a small percentage of carbon particle concentration of $\phi = 0.05$ is added, the speed decreases, but the wavy phenomenon increased due to the phase difference, as shown in Figs. 5b and 6b. When the percentage of concentration increased to $\phi = 0.1$ or $\phi = 0.2$ and with the surface roughness, the velocity decreased significantly, as shown in Figs. 5c, 6c, and d.

By increasing the electric and the magnetic fields to $S = 50, Ha = 1$, as shown in Fig. 7, the flow increases in the middle region and decreases as we approach the wall's region, with an increase in velocity also occurring when particles are present. Layers of liquids are greatly affected by the Lorentz force, which increases when the Hartmann number (Ha) increases and in the presence of a tangential electric field S. The impact of this force is observed and is clearly shown in the previous figures. Fig. 8 depicts the variance of the velocity distribution at $S = 50$, $Ha = 0.5$, in both cases of corrugated/flat channel; one can observe, a reduction in the velocity at the center of the channel occurs due to the corrugation of the walls and reduces more in the presence of the nanoparticles. Physically, the presence of nanoparticles raises the fluid viscosity which reflected in the velocity by the reduction.

Fig. 9 shows the average velocity ω_m as the Hartman number Ha increases if the phase difference between the two walls is 0° (represented by the solid lines) and 180° (represented by the dashed lines). The mean velocity ω_m gradually reaches a maximum value as the Hartman number increases from 1.0 to 1.5 and then decreases reduces to a minimum value. Furthermore, the presence of nanoparticles reduces the mean velocity of the flow, particularly in the opposite phase channel.

3.2. Effect of wall roughness on flow temperature in the presence of nanofluidic particles

After deriving the heat Eq. (56) and using Maxwell's model with n as the parameter, the structural coordination of nanoparticles is given by $3/\xi$, where ξ is the spherically of nanoparticles. For spherical nanoparticles, $\xi = 1$ or $n = 3$, but the (H-C) model reduces nanoparticles to cylindrical shapes, with $\xi = 0.5$ or $n = 6$. The goal of the temperature study is to examine the effect of the different models of heat conduction mentioned. Fig. 10 shows the behavior of both the transverse magnetic and electric fields. It helps to regulate the temperature of the flowing

liquid. The thermal distribution shows that as the number of nanoparticles increases, the temperature increases. When the transverse magnetic and electric fields are increased $S = 25, Ha = 0.5$, the degree increases when the nanoparticles are increased, as shown in Fig. 11. When studying the effect of nanoparticles on heat transfer, we observed that the rate of the increase of the Nusselt number Nu increases as the concentration of nanoparticles increases. Fig. 12 shows the Nusselt number with increasing Nu of Hartmann number Ha. If the phase difference between the two walls is 0° (represented by the solid lines) and 180° (represented by dashed line), the electric and magnetic fields control the rate of heat transfer. It is observed that from the energy equation, the joule temperature increases as the transverse magnetic and electric fields increase.

Therefore, the temperature spread is further increased by increasing the transverse magnetic and electric fields. Fig. 13 shows the effect of nanoparticles on heat generation/absorption ψ, when the phase difference between the two walls is 0° (represented by the solid lines) and 180° (represented by dashed lines), the rate of increase of the Nusselt number Nu increases when the concentration of nanoparticles increases.

Table 5 shows the numerical values of heat transfer rates for changes in the nanoparticle concentration. A comparison of the Maxwell model, the H-C model, and the Xue model is made in this table. The H-C model has the lowest heat transfer rate by 5.19% at 0.2 concentration. The heat transfer rate of the Maxwell model is higher than that of the H-C model by 15.01% at 0.2 concentrations. The Xue model increases the heat transfer rate by 23.33% at 0.2 concentrations. We also note that all three models, increasing the fracture size in the nanotubes increases the heat transfer rate. When we compare the Xue model with the other models, we note that the heat transfer rate predicted by the Xue model is higher than that by the other models. These results agree with previous findings by [11]. Fig. 14 presents a comparison between the three models of thermal characteristics suggested in this study, it is clear that the rate of heat transfer for Xue's model is the highest one by 84.78 % compared with Maxwell's model and by 133.56 % compared with the H-C model.

4. Conclusion

The flow and heat rate effects of SWCNTs, as well as wall surface roughness, were studied through a fine corrugated channel in the presence of magnetic and electric fields at a constant pressure gradient, and the following conclusions were reached.

- Due to the phase difference between the two walls, the speed and temperature distribution depend on the shape of the channel wall.
- When the corrugation increases, the phenomenon of ripple speed and temperature distribution becomes apparent.
- One can observe that the velocity distribution decreases as the concentration increases due to an increase in fluid viscosity.
- The impact of the transverse electric field (S) on the velocity contour is visible. It is observed that increasing the transverse electric field improves the fluid velocity and makes the wavy phenomenon of the flow is more visible.
- The addition of SWCNTs, reduces the fluid velocity at the center of the channel by providing resistance to the fluid motion.
- When the transverse electric field is increased, there is a spread and temperature rise.
- The concentration of SWCNTs influence enhances the rate of heat transfer.
- The rate of increase of the Nusselt number Nu increases when the concentration of nanoparticles increases.
- Heat generation/absorption increases as the transverse magnetic and electric fields increase with the change in the concentration of SWCNTs.
- Xue's model has the highest heat transfer rate compared to the Maxwell and H-C models.

Funding

Not applicable.

Ethical approval

This article does not contain any studies with human participants or animals performed by any of the authors.

CRediT authorship contribution statement

Ahmed Y. Sayed: Conceptualization, Validation, Writing - Reviewing and Editing.

Shaaban I. Ahmed: Data curation, Writing - Original draft preparation and Methodology

Khaled. S. Mekheimer: Conceptualization, Methodology and Supervision

Mohamed S. Abdel-wahed: Methodology, Software, Validation and Reviewing

Declaration of competing interest

The authors declare that they have no competing interests.

Data availability

No data was used for the research described in the article.

Acknowledgements

We express our gratitude to the anonymous referees for their constructive reviews of the manuscript and for helpful comments.

Appendix A

$$S_1{}^2 = \alpha^2 + \lambda^2 \tag{A-1}$$

$$S_2{}^2 = \alpha^2 + 4\lambda^2 \tag{A-2}$$

$$B_1 = Ha^2 \frac{A_2}{A_1^2} P_z + \frac{A_2^2}{A_1^2} Ha^3 S \tag{A-3}$$

$$B_2{}^2 = \lambda^2 + A^2 \tag{A-4}$$

$$B_3{}^2 = 4\lambda^2 + A^2 \tag{A-5}$$

$$B_4 = \frac{\left(A^2 Q + B_1\right) Tanh[A]}{A} \tag{A-6}$$

$$g_1{}^{+}(y) = \frac{\text{Csch}[2\lambda]\text{Sin}[x\lambda]}{\lambda^2 - B_2^2}\left(2\gamma\text{Cosh}[\lambda](\text{Sinh}[y\lambda] - \text{Csch}[B_2]\text{Sinh}[\lambda]\text{Sinh}[yB_2])B_4 - \left(\lambda^2 - B_2^2\right)(\text{Sinh}[(1+y)\lambda]B_5 + \text{Sinh}[\lambda - y\lambda]B_6)\right) \tag{A-7}$$

$$g_1{}^{-}(y) = \frac{1}{(-1+e^{4\lambda})\left(\lambda^2 - B_2^2\right)} e^{-y\lambda}\text{Sin}[x\lambda]\left(\left(-1+e^{2\lambda}\right)\gamma\left(-e^{\lambda}\left(1+e^{2y\lambda}\right) + e^{y\lambda}\left(1+e^{2\lambda}\right)\text{Cosh}[yB_2]\text{Sech}[B_2]\right)B_4 - 2e^{(2+y)\lambda}\left(\lambda^2 - B_2^2\right)(\text{Sinh}[(1+y)\lambda]B_5 - \text{Sinh}[\lambda - y\lambda]B_6)\right) \tag{A-8}$$

$$g_2{}^{+}(y) = \frac{(1+y)B_7 - (-1+y)B_8}{4} + \frac{\gamma\left(A^2 Q(1 - \text{Cosh}[Ay]\text{Sech}[A]) + (1 - \text{Cosh}[Ay]\text{Sech}[A])(B_1 - 2\text{Coth}[B_2]B_2B_4)\right)}{4A^2} \tag{A-9}$$

$$g_2{}^{-}(y) = \frac{(1+y)B_9 - (-1+y)B_{10}}{4} + \frac{\gamma\left(A^2 Q(1 - \text{Cosh}[Ay]\text{Sech}[A]) + (1 - \text{Cosh}[Ay]\text{Sech}[A])(B_1 - 2B_2B_4\text{Tanh}[B_2])\right)}{4A^2} \tag{A-10}$$

$$\begin{aligned} f^{+}(y) = {} & \frac{1}{4(-1+e^{8\lambda})\left(4\lambda^2 - B_3^2\right)}\left(A^2 Q\gamma\left(2e^{2\lambda}\left(-1+e^{4\lambda}\right)\text{Cosh}[2y\lambda] - \left(-1+e^{8\lambda}\right)\text{Cosh}[yB_3]\text{Sech}[B_3]\right) + 2e^{4\lambda}\left(\gamma(2\text{Cosh}[2y\lambda]\text{Sinh}[2\lambda]\right.\right. \\ & \left.\left. - \text{Cosh}[yB_3]\text{Sech}[B_3]\text{Sinh}[4\lambda])(B_1 - 2\text{Coth}[B_2]B_2B_4) - 2\left(4\lambda^2 - B_3^2\right)(\text{Sinh}[2(1+y)\lambda]B_7 + \text{Sinh}[2\lambda - 2y\lambda]B_8)\right)\right) \end{aligned} \tag{A-11}$$

$$\begin{aligned} f^{-}(y) = {} & \frac{1}{16\lambda^2 - 4B_3^2}\left(A^2 Q\gamma(\text{Cosh}[2y\lambda]\text{Sech}[2\lambda] - \text{Cosh}[yB_3]\text{Sech}[B_3]) - 2\text{Csch}[4\lambda]\left(4\lambda^2 - B_3^2\right)(\text{Sinh}[2(1+y)\lambda]B_9 + \text{Sinh}[2\lambda - 2y\lambda]B_{10})\right. \\ & \left. + \gamma(\text{Cosh}[2y\lambda]\text{Sech}[2\lambda] - \text{Cosh}[yB_3]\text{Sech}[B_3])(B_1 - 2B_2B_4\text{Tanh}[B_2])\right) \end{aligned} \tag{A-12}$$

$$B_5 = \frac{\gamma B_1(-A + Tanh[A]) + A^2(A\delta + Q\gamma Tanh[A])}{A^3} \tag{A-13}$$

$$B_6 = \frac{\gamma B_1(A - Tanh[A]) - A^2(A\delta + Q\gamma Tanh[A])}{A^3} \tag{A-14}$$

$$B_7 = \frac{1}{2}(-Q\gamma - \delta) - \frac{\text{Csch}[2\lambda]\left(2\gamma\text{Cosh}[\lambda](\lambda\text{Cosh}[\lambda] - \text{Coth}[B_2]\text{Sinh}[\lambda]B_2)B_4 - \lambda\left(\lambda^2 - B_2^2\right)(\text{Cosh}[2\lambda]B_5 - B_6)\right)}{\lambda^2 - B_2^2} \tag{A-15}$$

$$B_8 = \frac{1}{2}(-Q\gamma - \delta) - \frac{\gamma(\lambda\text{Coth}[\lambda] - \text{Coth}[B_2]B_2)B_4 + \lambda\text{Csch}[2\lambda](\lambda - B_2)(\lambda + B_2)(-B_5 + \text{Cosh}[2\lambda]B_6)}{\lambda^2 - B_2^2} \tag{A-16}$$

$$B_9 = \frac{1}{2}(-Q\gamma - \delta) - \frac{-2e^{2\lambda}\lambda\left(\lambda^2 - B_2^2\right)(\text{Cosh}[2\lambda]B_5 + B_6) + \gamma B_4\left(-(-1+e^{2\lambda})^2\lambda + (-1+e^{4\lambda})B_2\text{Tanh}[B_2]\right)}{(-1+e^{4\lambda})\left(\lambda^2 - B_2^2\right)} \tag{A-17}$$

$$B_{10} = \frac{1}{2}(-Q\gamma - \delta) + \frac{-2e^{2\lambda}\lambda\left(\lambda^2 - B_2^2\right)(B_5 + \text{Cosh}[2\lambda]B_6) + \gamma B_4\left((-1+e^{2\lambda})^2\lambda - (-1+e^{4\lambda})B_2\text{Tanh}[B_2]\right)}{(-1+e^{4\lambda})\left(\lambda^2 - B_2^2\right)} \tag{A-18}$$

References

[1] Choi SUS. Enhancing conductivity of fluids with nanoparticles. ASME Fluid Eng. Division 1995;231:99–105.

[2] Khanafer K, Vafai K, Lightstone M. Buoyancy-driven heat transfer enhancement in a two-dimensional enclosure utilizing nanofluids. Int J Heat Mass Transf 2003;46 (19):3639–53.

[3] Kakaç S, Pramuanjaroenkij A. Review of convective heat transfer enhancement with nanofluids. Int J Heat Mass Transf 2009;52(13–14):3187–96.

[4] N. S. Wahid N. M. Arifin M. Turkyilmazoglu M. E. H. Hafidzuddin N. A. Abd Rahmin n.d. MHD hybrid Cu-Al2O3/water nanofluid flow with thermal radiation and partial slip past a permeable stretching surface: analytical solution, J Nano Res, 1661-9897, Vol. 64, 75-91.

[5] Turkyilmazoglu M. Nanofluid flow and heat transfer due to a rotating disk. Comput Fluids 2014;94:139–46.

[6] Elsaid EM, Abdel-wahed MS. Impact of hybrid nanofluid coolant on the boundary layer behavior over a moving cylinder: numerical case study. case studies inThermalEngineering 2021;25:100951.

[7] Abbasi FM, Hayat T, Ahmad B, Chen GQ. Peristaltic motion of a non-newtonian nanofluid in an asymmetric channel. Z Naturforsch 2014;69(8–9):451–61.

[8] Sayed AY, Abdel-wahed MS. Entropy analysis for an MHD nanofluid with a microrotation boundary layer over a moving permeable plate. Eur Phys J Plus 2020;135:106.

[9] Elsaid EM, Abdel-wahed MS. MHD mixed convection Ferro Fe3O4/Cu-hybrid-nanofluid runs in a vertical channel. Chin J Phys 2022;76:269–82.

[10] Elsaid EM, Abdel-wahed MS. Mixed convection hybrid-nanofluid in a vertical channel under the effect of thermal radiative flux. case studiesThermal Engineering 2021;25:100913.

[11] Hayat T, Abbasi FM, Ahmad B. Mixed convective peristaltic flow of carbon nanotubes submerged in water using different thermal conductivity models. Comput Methods Programs Biomed 2016;135:141–50.

[12] Abdel-wahed MS, Sayed AY. Hybrid/mono-carbon nanotubes–water flow in a peristaltic curved channel with viscous dissipation. Eur Phys J Plus 2021;136:979.

[13] Chakraborty S, Paul D. Microchannel flow control through a combined electromagnetohydrodynamic transport. J Phys D Appl Phys 2006;39(24): 5364–71.

[14] Anuar NS, Bachok N, Turkyilmazoglu M, Arifin NM, Rosali H. Analytical and stability analysis of MHD flow past a nonlinearly deforming vertical surface in carbon nanotubes. Alex Eng J 2020;59:497–507.

[15] Liu Y, Jian Y. Electroviscous effect on electromagnetohydrodynamic flows of Maxwell fluids in parallel plate microchannels. Appl Math Mech 2019;40(10): 1457–70.

[16] Xue QZ. Model for thermal conductivity of carbon nanotube-based composites. Phys B Condens Matter 2005;368(1–4):302–7.

[17] Zhao GP, Jian YJ, Li FQ. Electromagnetohydrodynamic flow and heat transfer of nanofluid in a parallel plate microchannle. J Mech 2017:115–24.

[18] Duwairi H, Abdullah M. Thermal and flow analysis of a magneto-hydrodynamic micropump. Microsyst Technol 2006;13(1):33–9.

[19] Yoon MS, Park JS, Hyun JM. Magnetohydrodynamics flow over a rapidly rotating axisymmetric wavy disk. Fluid Dyn Res 2011;43(4):041405.

[20] Buren M, Jian Y, Chang L. Electromagnetohydrodynamic flow through a microparallel channel with corrugated walls. J Phys D Appl Phys 2014;47(42): 425501.

[21] Andreozzi A, Manca O, Nardini S, Ricci D. Forced convection enhancement in channels with transversal ribs and nanofluids. Appl Therm Eng 2016;98:1044–53.
[22] Si D, Jian Y. Electromagnetohydrodynamic (EMHD) micropump of Jeffrey fluids through two parallel microchannels with corrugated walls. J Phys D Appl Phys 2015;48(8):085501.
[23] Rashid M, Shahzadi I, Nadeem S. Corrugated walls analysis in microchannels through porous medium under electromagnetohydrodynamic (EMHD) effects. Results Phys. 2018;9:171.
[24] Abo-Elkhair RE, Mekheimer KS, Moawad AMA. Combine impacts of electrokinetic variable viscosity and partial slip on peristaltic MHD flow through a micro-channel". Iran J Sci Technol Trans A Sci 2019;43(1):201–12.
[25] Liu Y, Jian Y, Tan W. Entropy generation of electromagnetohydrodynamic (EMHD) flow in a curved rectangular microchannel. Int J Heat Mass Transf 2018;27: 901–13.
[26] Rashid M, Nadeem S. EMHD flow through microchannels with corrugated walls in the presence of nanofluid. Can J Phys 2019;97(7):701–20.
[27] Reza M, Rana A, Shit GC. Thermo-fluidic transport of electromagnetohydrodynamic flow in a corrugated porous medium microchannel. Eur Phys J Plus 2021;136(5):496.
[28] Yang RJ, Fu LM, Lin YC, Crosser OK. Electroosmotic flow in micro channels. J Colloid Interface Sci 2001;239:98–105.
[29] Masliyah JH, Bhattacharjee S. Electrokinetic and colloid transport phenomena. Hoboken, NJ, USA: John Wiley & Sons Inc; 2006.
[30] Maxwell JCA. Treatise on electricity and magnetism. Cambridge: Cambridge University Press; 2010.
[31] Hamilton RL, Crosser OK. Thermal conductivity of heterogeneous two-component systems. Ind Eng Chem Fundam 1962;1(3):187–91.